Cancer Research

Serial Transcriptome Analysis and Cross-Species Integration Identifies *Centromere-Associated Protein E* as a Novel Neuroblastoma Target

Naomi J. Balamuth[1], Andrew Wood[1], Qun Wang[1], Jayanti Jagannathan[1], Patrick Mayes[1], Zhe Zhang[2], Zhongxue Chen[2], Eric Rappaport[3], Joshua Courtright[1], Bruce Pawel[4], Barbara Weber[6], Richard Wooster[6], Eric O. Sekyere[7], Glenn M. Marshall[7], and John M. Maris[1,5]

Abstract

Cancer genomic studies that rely on analysis of biopsies from primary tumors may not fully identify the molecular events associated with tumor progression. We hypothesized that characterizing the transcriptome during tumor progression in the TH-*MYCN* transgenic model would identify oncogenic drivers that would be targetable therapeutically. We quantified expression of 32,381 murine genes in nine hyperplastic ganglia harvested at three time points and four tumor cohorts of progressively larger size in mice homozygous for the TH-*MYCN* transgene. We found 93 genes that showed a linearly increasing or decreasing pattern of expression from the preneoplastic ganglia to end stage tumors. Cross-species integration identified 24 genes that were highly expressed in human *MYCN*-amplified neuroblastomas. The genes prioritized were not exclusively driven by increasing Myc transactivation or proliferative rate. We prioritized three targets [*centromere-associated protein E* (*Cenpe*), *Gpr49*, and *inosine monophosphate dehydrogenase type II*] with previously determined roles in cancer. Using siRNA knockdown in human neuroblastoma cell lines, we further prioritized *CENPE* due to inhibition of cellular proliferation. Targeting *CENPE* with the small molecular inhibitor GSK923295 showed inhibition of *in vitro* proliferation of 19 neuroblastoma cell lines (median IC_{50}, 41 nmol/L; range, 27–266 nmol/L) and delayed tumor growth in three xenograft models (P values ranged from $P < 0.0001$ to $P = 0.018$). We provide preclinical validation that serial transcriptome analysis of a transgenic mouse model followed by cross-species integration is a useful method to identify therapeutic targets and identify CENPE as a novel therapeutic candidate in neuroblastoma.

Cancer Res; 70(7); 2749–58. ©2010 AACR.

Introduction

Neuroblastoma is a pediatric cancer that arises from the developing sympathetic nervous system. Forty percent of cases present with a "high-risk" phenotype characterized by wide dissemination at diagnosis, unfavorable biology, and a high risk of relapse and treatment failure (1). Despite intensification of chemoradiotherapy, high-risk tumors historically have overall survival under 40% (2, 3). Further intensification risks adding negligible benefit at a significant cost (4, 5). A phase III trial targeting the ganglioside GD2 glycolipid, with chimeric monoclonal antibody (ch14.18) and cytokines, recently reported the first substantive improvement in survival by reducing relapse by 20% in high-risk disease (6). This suggests that incorporation of targeted therapeutics may improve treatment outcomes for children with high-risk neuroblastoma.

High-risk neuroblastomas acquire copy number aberrations that are distinct from low- and intermediate-risk cases, suggesting regions of recurrent somatic alterations harbor candidate genes (7–10). The seminal example of this is *MYCN* oncogene amplification, which is highly predictive for adverse outcome (11, 12), but MYCN is not yet pharmacologically tractable. An ongoing genome-wide association study has identified multiple single-nucleotide polymorphisms (13, 14) and copy number variations (15) associated with sporadic neuroblastoma. Total attributable risk from these loci remains modest. Genome-wide linkage analysis of familial neuroblastoma pedigrees identified germline mutations in anaplastic lymphoma kinase (*ALK*) as the major familial neuroblastoma predisposition gene (16). Whereas inhibition of ALK is a highly attractive

Authors' Affiliations: [1]Division of Oncology and Center for Childhood Cancer Research, Children's Hospital of Philadelphia, Department of Pediatrics, University of Pennsylvania; [2]Center for Biomedical Informatics and [3]Department of Pediatrics, Children's Hospital of Philadelphia; [4]Department of Pathology, Children's Hospital of Philadelphia and Department of Pathology and Laboratory Medicine, University of Pennsylvania School of Medicine; [5]Abramson Family Cancer Research Institute, University of Pennsylvania School of Medicine, Philadelphia, Pennsylvania; [6]GlaxoSmithKline, King of Prussia, Pennsylvania; and [7]Children's Cancer Institute Australia and Sydney Children's Hospital, Sydney, Australia

Note: Supplementary data for this article are available at Cancer Research Online (http://cancerres.aacrjournals.org/).

N.J. Balamuth, A. Wood, and Q. Wang contributed equally to this work.

Corresponding Author: John M. Maris, Center for Childhood Cancer Research, Division of Oncology, Children's Hospital of Philadelphia, CTRB 3060, 3501 Civic Center Boulevard, Philadelphia, PA 19104-4318. Phone: 215-590-5244; Fax: 267-426-0685; E-mail: maris@chop.edu.

doi: 10.1158/0008-5472.CAN-09-3844

therapeutic target for this subset of patients, tractable molecular targets have not been identified for the majority of high-risk patients.

Here, we use a transgenic model of high-risk neuroblastoma to discover somatic transcriptional alterations in murine tumors that seem to be critical for progression. By filtering this list with both human neuroblastoma transcriptional data and matching the resultant gene list with anticancer drugs currently in development, we show the utility of this strategy in the prioritization of early-phase clinical trial planning.

Materials and Methods

Homozygous TH-MYCN$^{+/+}$ mice. TH-*MYCN* mice bred to homozygosity (TH-*MYCN*$^{+/+}$) develop tumors with near complete penetrance (17–19). TH-*MYCN*$^{+/+}$ mice were sacrificed at birth, day 7, or day 14 to harvest superior cervical and celiac sympathetic ganglia. Ultrasonography (Vevo770 Visual Sonics) was performed thrice per week. Mice were sacrificed when tumors were within one of four predetermined size ranges (six mice per cohort). Specimens were cryopreserved for nucleic acid extraction or preserved in paraffin and ornithine carbamyl transferase for histologic evaluation. Mice were maintained under the protocols and conditions were approved by the Institutional Animal Care and Use Committee.

Immunohistochemistry. We stained with endothelial cell marker CD34 (Abcam, ab8158, Cambridge, MA) at 1:50 dilution to quantify vessels. Sections were incubated with a biotinylated goat anti-mouse secondary antibody, and tertiary staining was with horseradish peroxidase–conjugated streptavidin. The immune complex was visualized by using liquid 3,3′-diaminobenzidine as a chromagen (DAKO, LSAB 2 System, K0673, North American, Inc.).

Microarray. RNA was extracted from 10-μm frozen sections using Qiagen RNeasy Micro kit (Qiagen). Tumor total RNA (76 ng to 1.6 μg) was used to generate cDNA targets that were hybridized to the Applied Biosystems Mouse Genome Survey Microarray version 1.0, and ganglia samples (which became available later in the experimental plan) were hybridized to version 2.0 of the array. Two tumors were hybridized to both microarray versions for quality control. All microarray data are available at the National Center for Biotechnology Information (NCBI) web site (http://www.ncbi.nlm.nih.gov/geo/query/acc.cgi?acc=GSE17740).

Differential expression in ganglia and tumor progression. We analyzed tumor and ganglia data sets separately, as they were analyzed on different microarray versions, and ganglia specimens required additional genome amplification before hybridization. Transcripts were excluded (*a*) if they were not present on both microarray versions, (*b*) if they had no human orthologues, or (*c*) if transcripts were not expressed in at least three tumor specimens within any cohort. To identify genes with serially increasing or decreasing expression across the ganglia and tumor samples, we calculated nonparametric Spearman's correlation coefficients for each transcript. We used a permutation test to evaluate the false discovery rate of identified genes.

Cross-species integration. We carried out cross-species integration to identify transcripts that were overexpressed with murine neuroblastoma progression and human high-risk *MYCN*-amplified neuroblastomas. We tested human gene expression by comparing 28 low-risk and 20 *MYCN*-amplified high-risk neuroblastoma transcriptomes, previously assayed using the Human Genome U95v2 expression microarray platform (http://www.ncbi.nlm.nih.gov/geo/query/acc.cgi?acc=GSE3960) (20). The murine genes were mapped to Affymetrix U95 probe sets using the NCBI Homologene database. Genes with concordant overexpression in murine and human neuroblastomas proceeded to manual curation prioritizing druggable targets based on literature review. PANTHER classification system was used to classify biological function of genes with concordant expression (21).

Quantitative reverse transcription–PCR. Real-time quantitative reverse transcription–PCR (RT-PCR) was performed on TH-*MYCN*$^{+/+}$ tumors (Applied Biosystems). Relative expression of target genes was determined by normalization to β-2-microglobulin, TATA box binding protein, and hypoxanthine phosphoribosyltransferase using a standard curve. All experiments were performed in triplicate.

MYC transcriptional activity during tumor progression. We evaluated expression of the murine *Mycn* and *Mycc* and human *MYCN* during tumor progression using quantitative RT-PCR. We quantified Myc transcriptional activity using a clinically validated *a priori* defined gene expression signature (22) based on the Myc target gene database (http://www.myccancergene.org/index.asp) (23). High Myc transcriptional activity was indicated by upregulation or downregulation of *Mycc, Mycn*, and *Mycl* target genes.

siRNA validation. Functional validation of manually curated genes in a human neuroblastoma-derived cell line (NB1643) was performed using transient transfection of siRNA against *tumor-associated calcium signal transducer-1* (*TACSTD1*), *inosine monophosphate dehydrogenase type II* (*IMPDH2*), *GPR49*, and *centromere-associated protein E* (*CENPE*; Dharmacon, Thermo Scientific). *CENPE* siRNA knockdown was also performed in NB-EBc1, Kelly, SKNAS, and NGP. Cell proliferation was monitored using the RT-CES (ACEA Biosciences), which measures substrate adherent growth in real time, as described previously (24). Each experiment was performed in triplicate.

Cell cycle analyses. Cells were seeded at 50% confluence and cultured overnight to allow cell attachment. Cells were treated with inhibitor 24 h after seeding. At each treatment, time point media were removed and cells were harvested using 0.05% Trypsin-EDTA. Media and trypsin fractions were then combined and spun. Cells were fixed with ice-cold ethanol overnight. Membranes were permeabilized by incubating in phosphate–citric acid buffer for 5 min. Cells were spun and incubated with propidium iodide (50 μg/mL) and RNase A (250 μg/mL) for 30 min and analyzed by flow cytometry using a FACSCalibur (BD Bioscience).

Pharmacologic* CENPE *inhibition. *In vitro* activity of GSK923295 dissolved in DMSO was evaluated in 19 neuroblastoma cell lines using the RT-CES system. IC_{50} was

calculated from the area under the curve across a four-log dose range (1–10,000 nmol/L).

Xenograft studies. CB17 *scid* mice (Taconic Farms) were used to propagate s.c. implanted neuroblastoma tumors. Tumor diameters were measured using calipers. Tumor volumes were calculated using the formula, $(\pi/6)$ * diameter^3. Once tumor volume exceeded 200 mm^3, mice were randomized (n = 10 per arm) to receive either 125 mg/kg i.p. GSK923295 or vehicle (96% acidified water, 2% DMAC, 2% CREM) for a total of six doses using a 3 d on–4 d off–3 d on regimen.

Proliferative signature during tumor progression. We used an *a priori*–defined "proliferative signature" that identified genes that are upregulated in rapidly proliferating cells, both malignant and nonmalignant (25). We compared the distribution of nonparametric Spearman's correlation

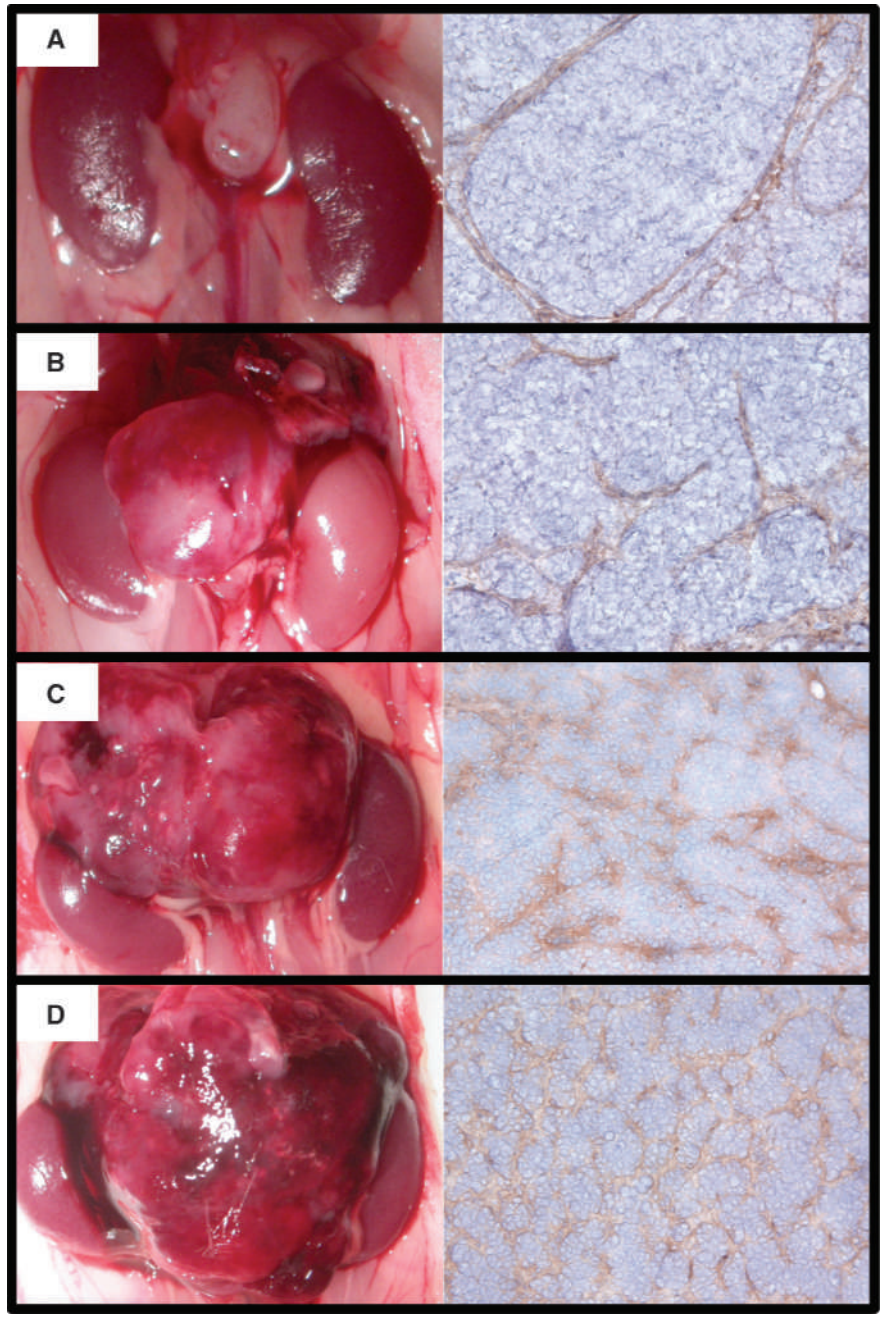

Figure 1. Harvested murine neuroblastomas represented clinically relevant stages of disease. Ultrasonography was used to monitor tumor growth. Tumors were harvested within four predetermined cohorts (n = 6/cohort). Group A tumors were harvested once detected on ultrasound (median, 0.08 ± 0.02 g) and were macroscopically avascular with scant vascularity on CD34 staining (A). Group B tumors (0.35 ± 0.09 g) displaced local structures and showed increased vascularity (B), but neither group A or group B tumors showed invasion of vasculature or metastases. Group C tumors (0.94 ± 0.22 g) showed local invasion (C), but not metastasis, although five of six tumors had intratumoral invasion of vasculature. Group D (2.01 ± 0.59 g) showed extensive local invasion (D) and intratumoral invasion of vasculature, with distant metastases in three of six animals. Groups C and D tumors showed increasing vascularity, which was grossly disorganized in the group D tumors. CD34 immunohistochemistry images, 200×.

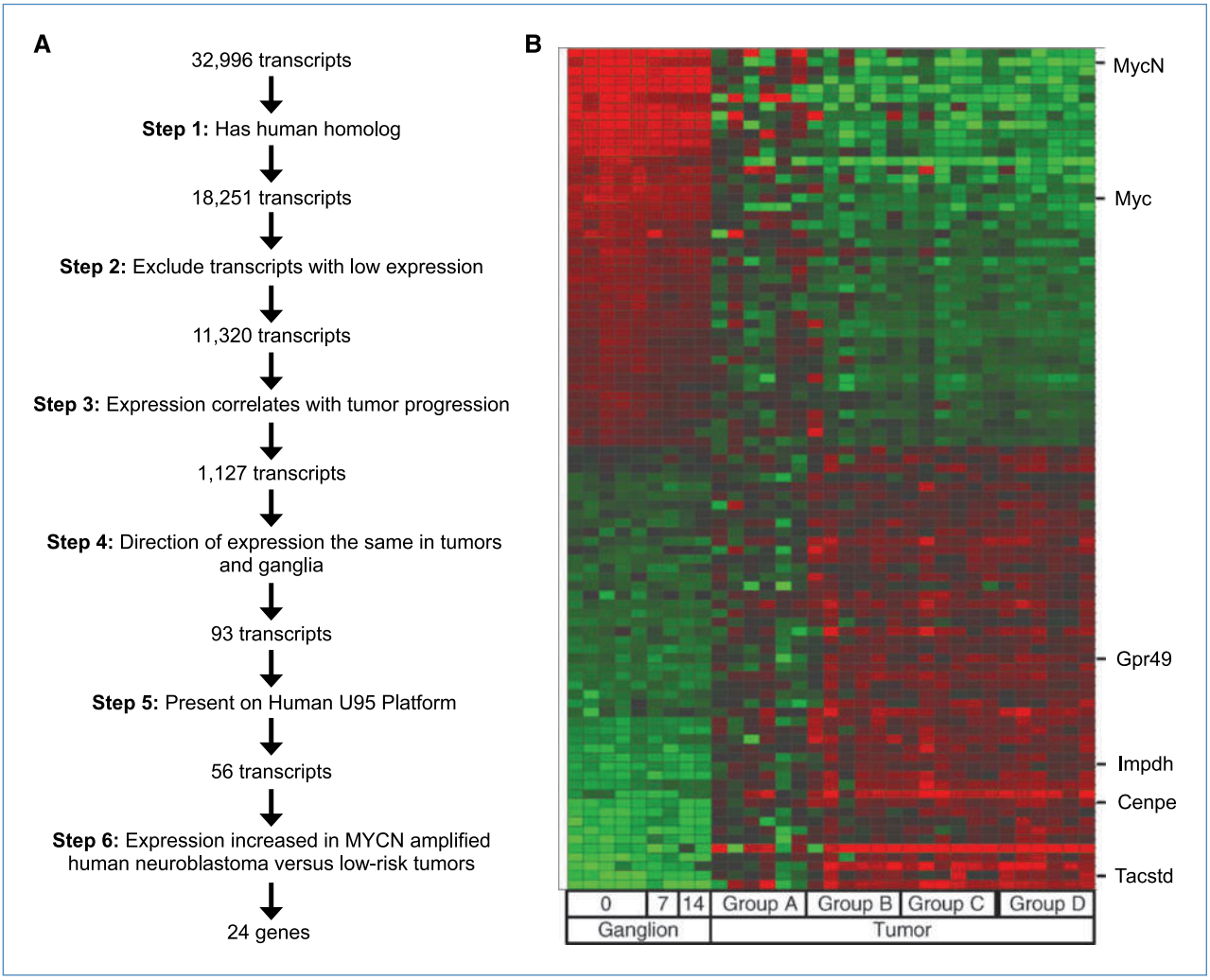

Figure 2. A, algorithm for identifying 24 candidates from ~32,000 transcripts. Transcripts showing a continuous increase or decrease in expression at clinically relevant stages of tumor progression and in hyperplastic ganglia at days 0, 7, and 14 were identified using Spearman's method. Microscopic ganglia required an additional round of amplification, so they were analyzed separately. Of the 93 transcripts, cross-species integration was used to prioritize 24 biologically important genes that were overexpressed in human high-risk MYCN-amplified neuroblastomas. B, heat map representation of 93 differentially expressed murine genes. Samples are grouped into ganglion samples (days 0, 7, and 14) and tumor samples (groups A–D) along the *X* axis. The 93 murine transcripts showing the most significant differential expression are shown along the *Y* axis, with red indicating greater expression and green indicating less expression. Four genes selected for functional evaluation are indicated. Note that murine Mycc and Mycn showed decreased expression with tumor progression. The full 93 gene set is described in Supplementary Table S2.

coefficients of the "proliferative signature" transcripts to murine transcripts with human orthologues that were not contained within the proliferative signature.

Results

Modeling tumor progression. We sacrificed TH-*MYCN*$^{+/+}$ mice at day 0 (n = 5), day 7 (n = 2), and day 14 (n = 2) of life to harvest sympathetic ganglia containing foci of neuroblast hyperplasia. To model progression of macroscopic tumors, we monitored tumor growth in TH-*MYCN*$^{+/+}$ mice using ultrasound. Mice were sacrificed when tumor dimensions were within predetermined ranges (Fig. 1). Increasing tumor volume on ultrasound corresponded to increasing tumor weight: group A, mean weight 0.08 ± 0.02 g; group B, 0.35 ± 0.09 g; group C, 0.94 ± 0.22 g; and group D, 2.01 ± 0.59 g. We confirmed that harvesting tumors at different sizes provides a model of neuroblastoma progression by comparing cohorts for macroscopic and histologic vascularity, locoregional invasion, infiltration of intratumoral vasculature, and metastases. The smallest tumors were asymptomatic and avascular and had no evidence of metastasis. With increasing tumor size, there was increasing displacement and invasion of local structures and increasing vascularity (Fig. 1A–D). The two larger tumor sizes (groups C and D) invaded tumor vasculature,

and in the largest tumors (group D), distant metastases were detected (Supplementary Table S1).

Identification of differentially expressed genes associated with neuroblastoma progression. We assayed each harvested sample with a murine-specific microarray. Our algorithmic approach is shown in Fig. 2A. The murine-specific microarray interrogated 32,381 genes, of which 18,251 genes had human orthologues. The exclusion of transcripts with low expression in any tumor cohort yielded 11,320 transcripts for further consideration. We next identified transcripts showing the strongest correlation of mRNA quantity to tumor progression using Spearman's method (Supplementary Table S2). Using a conservative false discovery rate of 0.05, we obtained 1,127 transcripts. We filtered the 1,127 candidates by determining which transcripts showed the same direction of expression in murine sympathetic ganglia across day 0, day 7, and day 14 of life. Of 1,127 candidates, 93 transcripts showed a consistent alteration in mRNA quantity (one-tailed $P \leq 0.01$) with progression from hyperplastic ganglia to advanced neuroblastomas (Fig. 2B; Supplementary Table S2).

Cross-species integration of gene expression. Of the 93 murine genes with differential expression, 56 had homologues present on the human microarray platform and 32 of these had increasing expression with tumor progression. We focused on genes with increasing expression, as potential oncogenes provide a more tractable therapeutic target than potential tumor suppressors. Of the 32 murine transcripts, we found 24 unique genes that were overexpressed in human high-risk *MYCN*-amplified neuroblastoma compared with low-risk nonamplified neuroblastomas (Supplementary Table S2). The 24 genes with concordant overexpression in murine and human *MYCN*-amplified neuroblastoma were classified using PANTHER biological function (21).

Manual curation of the 24 differentially expressed transcripts prioritized three genes with previously described roles in cancer and potential for therapeutic inhibition (*Gpr49, Impdh2*, and *Cenpe*). To act as a control for cross-species integration, we identified the transcript with the largest increase in expression across murine tumor progression that was not overexpressed in human *MYCN*-amplified neuroblastomas. This transcript was *Tacstd1* gene. Quantitative PCR was used to confirm that the three candidate transcripts and the control transcript had increased expression with tumor progression (Fig. 3A–D).

MYCN *transactivation did not increase with tumor progression.* To ensure that our candidate genes were not simply the result of the basal myc activity, we investigated whether the human *MYCN* transgene was driving alterations in gene expression with tumor progression. Human *MYCN* transgene expression increased with tumor progression, but murine *Mycn* and *Myc* showed a decrease in expression. Overall, the average expression of *MYCN, Mycc*, and *Mycn* remained unchanged from small avascular tumors to large metastasizing tumors (Fig. 4A). Myc transcriptional activity, as indicated by upregulation or downregulation of *Myc, Mycn*, and *Myc* target genes, did not show a significant increase with tumor progression (Fig. 4B). *Cenpe, Gpr49*, and *Impdh2* showed a significant linear increase in expression with tumor progression (Fig. 3A–D), but Myc transcriptional activity did not (Fig. 4B).

Transcripts with increased expression were not exclusively composed of genes involved in proliferation. Following

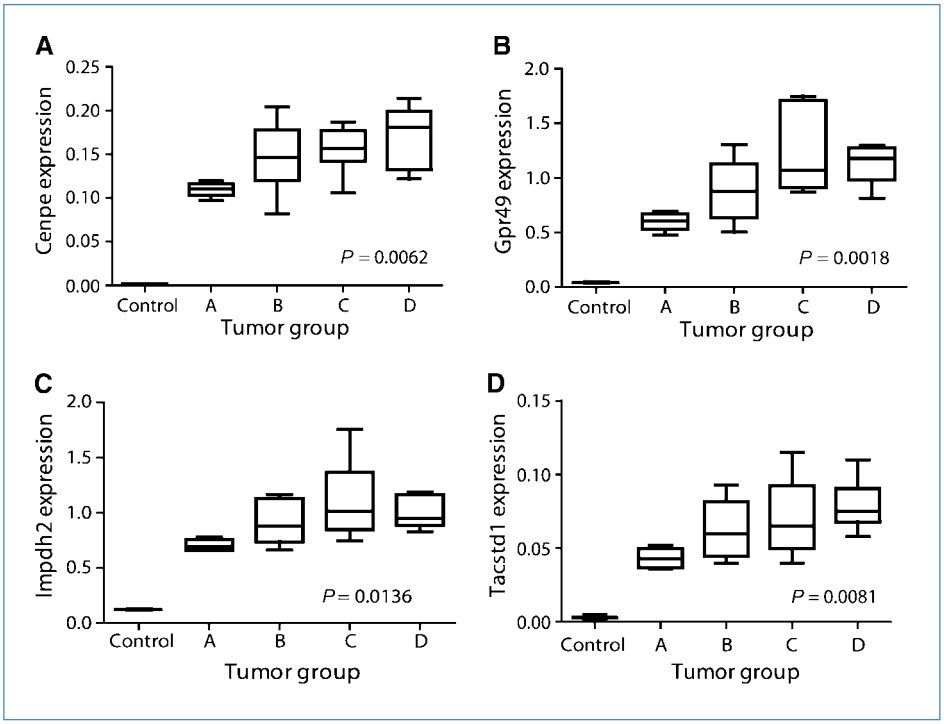

Figure 3. Prioritized transcripts showed increased expression with tumor progression, but Myc transcriptional activity did not increase. Real-time PCR confirmed that three genes prioritized using a literature search, *Cenpe* (A), *Gpr49* (B), and *Impdh2* (C), and the control gene not overexpressed in human *MYCN*-amplified neuroblastoma, *Tacstd1* (D), showed a significant linear increase in expression with tumor size.

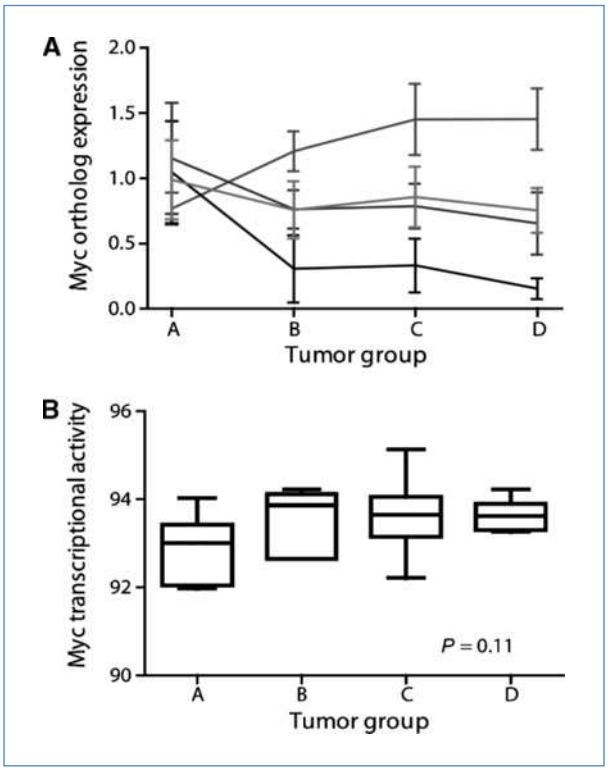

Figure 4. Gene expression signatures not driven by basal myc expression. A, murine neuroblastoma expression of human *MYCN* transgene mRNA (green) increased with tumor progression, whereas murine *Mycn* (black) and *Mycc* (blue) expression decreased. Overall, the average *MYCN, Mycn*, and *Mycc* expression did not increase with tumor progression (red). B, Myc transcriptional activity was quantified using a clinically validated *a priori*–defined gene expression signature (28) with a higher score indicating greater upregulation or downregulation of Myc targets. Myc transcriptional activity did not show a significant linear increase with tumor expression, suggesting that alterations in *MYCN* transactivation did not exclusively drive differential gene expression.

prioritization of the mitotic kinesin *Cenpe*, we sought to characterize if there was an excessive prevalence of other genes with cell cycle–related functions that were overexpressed in the larger murine tumors. Using an *a priori*–defined gene expression signature, we established that genes identified as being upregulated in rapidly dividing cells (25) were more likely to show upregulation in larger tumors compared with ~18,000 other murine transcripts (Supplementary Fig. S1). Among the 93 murine transcripts showing the greatest differential expression with tumor progression, there were 49 wherein expression increased with tumor progression. Of the 49 murine transcripts showing the greatest increase in expression with tumor progression, only four were directly involved with DNA replication, two were in the kinetochore, and two were involved with purine synthesis.

Transcription of MYC target genes did not increase with tumor progression. To ensure that our candidate genes were not simply the result of the basal myc activity, we investigated whether the human *MYCN* transgene was driving alterations in gene expression with tumor progression. Human *MYCN* transgene expression increased with tumor progression, but murine *Mycn* and *Myc* showed a parallel decrease in expression. Overall, the average expression of *MYCN, Mycc*, and *Mycn* remained unchanged from small avascular tumors to large metastasizing tumors (Fig. 4A).

To evaluate expression of Myc target genes in murine tumors, we used a predefined gene expression signature of Myc transcriptional targets shown to predict relapse and death from low-, intermediate-, and high-risk human neuroblastoma. This signature quantifies the overall pattern of transcription of Myc targets rather than limiting the evaluation to single transcripts. Overall transcription of the Myc target gene signature did not show a significant increase with tumor progression (Fig. 4B).

Functional validation prioritizes* CENPE *for further investigation. To functionally validate and prioritize the three candidate neuroblastoma targets (*CENPE, GPR49*, and *IMPDH2*), we performed siRNA knockdown in a *MYCN*-amplified human neuroblastoma-derived cell line (NB-1643). We also knocked down the control gene (*TACSTD1*), which was overexpressed with tumor progression but not overexpressed by human high-risk MYCN-amplified neuroblastomas. siRNA knockdown resulted in variable effects on cellular proliferation. Transient knockdown of *TACSTD1* resulted in no significant decrease in growth velocity when compared with a targeted control, *glyceraldehyde-3-phosphate dehydrogenase* (*GAPDH*; Fig. 5A). Knockdown of *GRP49* (Fig. 5B) and *IMPDH2* (Fig. 5C) showed modest inhibition of proliferation, but knockdown of *CENPE* resulted in the greatest inhibition prioritizing *CENPE* for further evaluation (Fig. 5D). Finally, to assure that the CENPE siRNA inhibition was not specific to the human neuroblastoma cell line NB1643, we performed additional transient siRNA knockdown experiments in three additional MCYN-amplified human neuroblastoma-derived cell lines (Kelly, NGP, and NBEbC1) as well as one nonamplified line (SKNAS). There was significant inhibition of cell growth in all three amplified lines, whereas the nonamplified line showed little effect (Supplementary Fig. S2C).

CENPE knockdown-induced suppression of neuroblastoma cell proliferation results from mitotic arrest. Following confirmation of knockdown by RT-PCR (Supplementary Fig. S2B), we examined cell cycle inhibition in two human neuroblastoma cell lines (SKNAS and NGP) using flow cytometry. At 24 hours, there was an accumulating cell population in the G_2-M phase of the cell cycle. Notably, there is no sub-2N population to suggest apoptotic cell death (Supplementary Fig. S2A).

***Pharmacologic inhibition of* Cenpe *results in antitumor activity* in vitro *and* in vivo.** We sought validation that pharmacologic CENPE inhibition was efficacious in preclinical models. A potent CENPE Inhibitor, GSK923295, showed broad efficacy against a panel of 19 human neuroblastoma-derived cell lines with an average growth IC_{50} of 41 nmol/L (range, 27–266 nmol/L; Supplementary Table S3). Growth IC_{50} did not correlate to cell line *MYCN* amplification status ($P = 0.51$), CENPE copy number gain ($P = 0.29$), *in vitro* cell line doubling time ($r = 0.41$, $P = 0.0805$), or *CENPE* mRNA expression as previously assayed by the Illumina Human-6 v2 expression BeadChip ($r = -0.12$, $P = 0.62$).

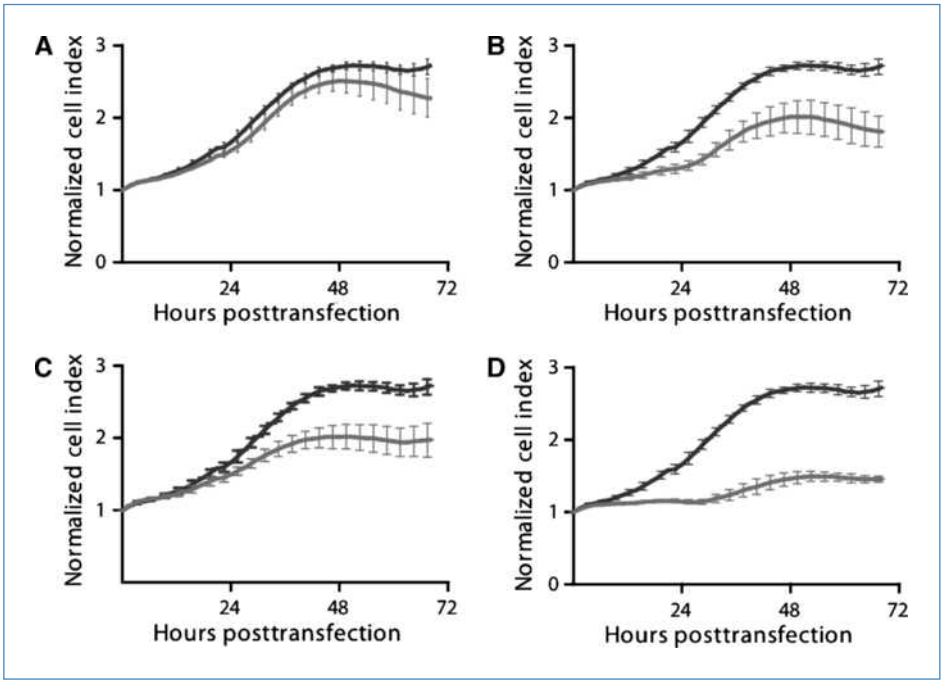

Figure 5. siRNA knockdown prioritizes *CENPE* for further functional evaluation. We monitored proliferation of NB-1643, a *MYCN*-amplified human neuroblastoma cell line, using the RT-CES microelectronic cell sensor system. A, the control gene *TACSTD1*, which was not overexpressed in human *MYCN*-amplified neuroblastomas, showed minimal inhibition of proliferation with knockdown. Inhibition was modest for *GPR49* (B) and *IMPDH2* (C). D, *CENPE* siRNA caused the greatest inhibition. The gene of interest is red, and *GAPDH* (negative control) is blue. All experiments performed in triplicate. Points, mean; bars, SEM. PLK (positive control) showed 100% cell kill at 72 h posttransfection in all cases.

We selected three cell lines with a spectrum of *in vitro* growth IC_{50} (NB-EBc1, 34 nmol/L; NB1643, 57 nmol/L; NB1691, 103 nmol/L) to assess *in vivo* GSK293295 activity. Xenografts of mice treated with GSK293295A showed significant tumor growth delay compared with the control arm (NB-EBc1, $P < 0.0001$; NB-1643, $P = 0.018$; NB-1691, $P = 0.0018$; Fig. 6). GSK293295A does not target murine *Cenpe* so no toxicity was seen, and a therapeutic index could not be estimated.

Discussion

Emerging evidence suggests that neuroblastoma initiation and progression occur due to a combination of inherited variants and mutations (13–16) and stepwise somatic accumulation of drivers (10, 26). Diagnostic specimens provide a snapshot at one time point and the molecular events associated with tumor evolution may not be fully identified. We hypothesized that characterizing the evolution of the neuroblastoma transcriptome at multiple time points would augment existing cancer gene discovery. We serially sacrificed TH-*MYCN* mice to obtain specimens to provide a model of human neuroblastoma progression. Using a transgenic system meant we could use cross-species integration to reduce the number of candidate genes before manual curation. Mouse tumors with chromosomal instability acquire genomic aberrations that are orthologous with their respective human cancers, suggesting that selection pressures are tissue specific

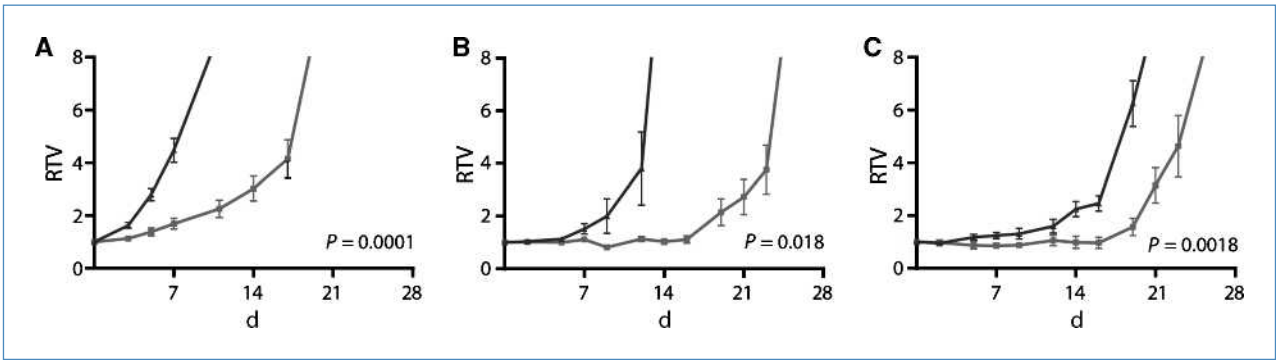

Figure 6. Pharmacologic *CENPE* inhibition caused tumor growth delay in three human neuroblastoma xenografts. Mice were randomized to receive either 125 mg/kg i.p. GSK923295 (red) or vehicle (blue; 96% acidified water, 2% DMAC, and 2% CREM). Relative tumor volume (RTV) is the measured tumor volume divided by the enrollment tumor volume displayed as mean ± SEM. Linear mixed effects analysis showed smaller relative tumor volume in the treatment arm in all three xenografts. A, NB-EBc1, $P = 0.0001$; B, NB-1643, $P = 0.018$; and C, NB-1691, $P = 0.0018$.

(27). Cross-species integration has been used with the transcriptome, as expression signatures of oncogenic *KRAS2* mutations were identified using cross-species integration transgenic and human cancers (28). We predicted that biologically relevant alterations in gene expression would also be conserved. By identifying commonalities in gene expression, we posited that we would be more likely to identify critical driver genes that could be inhibited therapeutically.

MYCN overexpression is responsible for tumor initiation in the TH-*MYCN* model, but it was unknown whether increasing *MYCN* transcriptional activity accounted for differential gene expression with tumor progression. Overall expression of Myc homologues and Myc transcriptional activity remained constant with tumor progression, suggesting that increasing *MYCN* transactivation was not exclusively driving alterations in gene expression. These findings are consistent with the hypothesis that the latent period before murine neuroblastoma initiation is due to the time needed to acquire cooperating mutations (17), which may contribute to differential gene expression. Following prioritization of the mitotic protein *CENPE*, we queried how many other genes identified had cell cycle–related functions. We established that genes upregulated in rapidly proliferating cells (25) showed greater upregulation with tumor progression than ~18,000 other murine transcripts. However, of the 93 murine genes with the greatest differential expression, 49 of those had increasing expression, and of those only four were directly involved with DNA replication, two were in the kinetochore, and two were involved with purine synthesis. Therefore, upregulation of the remaining transcripts was not a direct result of increased proliferative rate. These validations increase our confidence that we have not purely identified candidate genes that are artifacts of the model system but additional important functional mediators of tumorigenesis.

We identified 93 genes whose expression continuously increased or decreased across ganglia and tumor progression (Fig. 1; Supplementary Table S2). We used cross-species integration to reduce the number of transcript candidates by selecting those genes whose expression was greater in high-risk *MYCN*-amplified neuroblastomas relative to low-risk tumors without amplification of *MYCN* (Supplementary Table S2). The resultant 24 genes were prioritized based on whether we could inhibit them pharmacologically and identified three target genes. The G protein–coupled receptor (*GPR49/LGR5*) is overexpressed in carcinomas (31, 32). *IMPDH2* is an enzyme involved in purine synthesis. Functional validation using siRNA-mediated knockdown against two target candidates, *IMPDH2* and *GPR49*, resulted in moderate inhibition. siRNA-mediated knockdown caused low or no inhibition in the control gene *TACSTD1*, which was not overexpressed in human high-risk disease. It is possible that further analysis of the candidate transcripts in cell lines with differing genomic profiles or different model systems will establish a greater therapeutic benefit.

Knockdown of *CENPE* showed the greatest growth inhibition *in vitro*. CENPE is a kinesin motor protein included in the kinetochore protein complex, whose motor activity is required for correct chromosomal alignment during metaphase. To satisfy the spindle assembly checkpoint before anaphase (33, 34), *CENPE* must be simultaneously bound to both the kinetochore and spindle microtubule to prevent asymmetrical separation of sister chromatids (34). We focused our initial studies on *CENPE* as knockdown showed the greatest inhibition, mitotic kinesins are druggable targets, and inhibition of mitosis is a proved cancer paradigm. The traditional microtubule-binding drugs, *Vinca* alkaloids and taxanes, have documented antitumor activity against a broad spectrum of malignancies, including neuroblastoma. Microtubule disruption during mitosis inhibits the mitotic spindle resulting in mitotic arrest in tumor cells, followed in some cases by cell death. CENPE's known functions are restricted to cell division, suggesting that on-target toxicity will be limited to dividing cells, theoretically providing an advantageous therapeutic index over microtubule binding agents.

GSK923295 is a potent and selective small molecule inhibitor of human *CENPE* with a Ki of 3.2 nmol/L. It directly inhibits microtubule-stimulated ATPase activity of the human *CENPE* motor domain, resulting in irreversible binding of *CENPE* to microtubules and mitotic arrest. GSK923295 has shown *in vitro* and *in vivo* activity against a broad spectrum of malignancies. A phase I study of GSK923295 is currently nearing completion in adults with refractory solid cancers, and early results have been promising in terms of safety (35). The identification of *CENPE* in our cross-species integrative genomics study of transcriptome evolution suggests that it is also a rational target for neuroblastoma. We show that GSK923295 has significant activity against a panel of human neuroblastoma-derived cell lines *in vitro* and *in vivo*. Our findings suggest that a transgenic model recapitulating the *MYCN*-amplified subset of neuroblastoma can discover downstream oncogenic mediators common to tumors without *MYCN* amplification. Importantly, this inhibitor is relatively inactive against murine *Cenpe*, meaning we were unable to test the inhibitors against TH-*MYCN* neuroblastomas used for target discovery nor could we estimate a therapeutic index in xenograft or transgenic models. Interestingly, although the identification of CENPE included differential expression between MYCN-amplified and nonamplified human tumors, GSK023295 activity did not correlate with MYC status or CENPE expression. This suggests the presence of as yet unidentified variables important in predicting CENPE activity.

The mechanism for increased *CENPE* expression in neuroblastoma remains unclear. *CENPE* is not a known Myc target gene (http://www.myccancergene.org/index.asp). We analyzed *CENPE* copy number on 599 primary neuroblastoma tumors previously assayed using the Illumina HumanHap550 SNP microarray. Relative copy number loss occurred in 66 of 599 (11%) and gain in 48 of 599 (8%) of tumors. Copy number gains were mostly whole chromosome gains and were not significantly associated with *CENPE* overexpression ($P = 0.89$). This indicates that *CENPE* would be unlikely to have been prioritized as target using genomic data obtained at diagnosis, but it was identified through serial transcriptomic analysis of neuroblastoma progression. This suggests that serial transcriptome analysis can augment existing integrative genomic strategies.

In summary, we used serial transcriptome analysis and cross-species integration to identify molecular targets associated with tumor progression. Our gene set includes many targets with no previously established role in tumor progression and numerous candidates suitable for pathway analysis. Future follow-up studies with these genes may uncover novel biological roles in neuroblastoma oncogenesis. The focus of this study was to identify molecular targets from this gene set that have the potential to be quickly translated into therapies for high-risk neuroblastoma. This led to the preclinical evaluation of a *CENPE* inhibitor that is currently in an adult phase I trial. Other genes identified in this study may prove to be equally strong candidates for therapeutic targeting. Likewise, analysis of transcripts with decreasing expression may aid identification of *bona fide* tumor suppressor genes, which are yet to be identified in sporadic neuroblastoma. Future studies will focus on the transcriptional and post-transcriptional regulation of *CENPE* expression in neuroblastoma cells. In conclusion, we have provided strong preclinical rationale that serial transcriptome profiling of a spontaneous tumor model with cross-species integration can identify and prioritize novel therapeutic targets in neuroblastoma. This strategy may have utility in other tumor types and further utility in neuroblastoma for target discovery.

Disclosure of Potential Conflicts of Interest

J.M. Maris: commercial research grant. The other authors disclosed no potential conflicts of interest.

Grant Support

NIH grants R01-CA78545 (J.M. Maris), R01-CA87847 (J.M. Maris), and P01 CA97323 (J.M. Maris); NH&MRC Australia (G.M. Marshall); Cancer Institute New South Wales (G.M. Marshall); Cancer Council New South Wales (G.M. Marshall); Alex's Lemonade Stand Foundation (J.M. Maris); a research collaborative agreement with GlaxoSmithKline; and Abramson Family Cancer Research Institute (J.M. Maris).

The costs of publication of this article were defrayed in part by the payment of page charges. This article must therefore be hereby marked *advertisement* in accordance with 18 U.S.C. Section 1734 solely to indicate this fact.

Received 10/18/2009; revised 01/19/2010; accepted 01/20/2010; published OnlineFirst 03/16/2010.

References

1. Maris JM, Hogarty MD, Bagatell R, Cohn SL. Neuroblastoma. Lancet 2007;369:2106–20.
2. Matthay KK, Villablanca JG, Seeger RC, et al, Children's Cancer Group. Treatment of high-risk neuroblastoma with intensive chemotherapy, radiotherapy, autologous bone marrow transplantation, and 13-*cis*-retinoic acid. N Engl J Med 1999;341:1165–73.
3. Berthold F, Boos J, Burdach S, et al. Myeloablative megatherapy with autologous stem-cell rescue versus oral maintenance chemotherapy as consolidation treatment in patients with high-risk neuroblastoma: a randomised controlled trial. Lancet Oncol 2005;6:649–58.
4. Oeffinger KC, Mertens AC, Sklar CA, et al. Chronic health conditions in adult survivors of childhood cancer. N Engl J Med 2006;355:1572–82.
5. Hobbie WL, Moshang T, Carlson CA, et al. Late effects in survivors of tandem peripheral blood stem cell transplant for high-risk neuroblastoma. Pediatr Blood Cancer 2008;51:679–83.
6. Yu AL, Gilman AL, Ozkaynak MF, et al. A phase III randomized trial of the chimeric anti-GD2 antibody ch14.18 with GM-CSF and IL2 as immunotherapy following dose intensive chemotherapy for high-risk neuroblastoma: Children's Oncology Group (COG) study ANBL0032 [abstract 10067z]. J Clin Oncol 2009;27.
7. Mosse YP, Diskin SJ, Wasserman N, et al. Neuroblastomas have distinct genomic DNA profiles that predict clinical phenotype and regional gene expression. Genes Chromosomes Cancer 2007;46:936–49.
8. Spitz R, Oberthuer A, Zapatka M, et al. Oligonucleotide array-based comparative genomic hybridization (aCGH) of 90 neuroblastomas reveals aberration patterns closely associated with relapse pattern and outcome. Genes Chromosomes Cancer 2006;45:1130–42.
9. Vandesompele J, Baudis M, De Preter K, et al. Unequivocal delineation of clinicogenetic subgroups and development of a new model for improved outcome prediction in neuroblastoma. J Clin Oncol 2005;23:2280–99.
10. Janoueix-Lerosey I, Schleiermacher G, Michels E, et al. Overall genomic pattern is a predictor of outcome in neuroblastoma. J Clin Oncol 2009;27:1026–33.
11. Brodeur G, Seeger RC, Schwab M, Varmus HE, Bishop JM. Amplification of N-myc in untreated human neuroblastomas correlates with advanced disease stage. Science 1984;224:1121–4.
12. Seeger RC, Brodeur GM, Sather H, et al. Association of multiple copies of the N-myc oncogene with rapid progression of neuroblastomas. N Engl J Med 1985;313:1111–6.
13. Capasso M, Devoto M, Hou C, et al. Common variations in BARD1 influence susceptibility to high-risk neuroblastoma. Nat Genet 2009;41:718–23.
14. Maris JM, Mosse YP, Bradfield JP, et al. Chromosome 6p22 locus associated with clinically aggressive neuroblastoma. N Engl J Med 2008;358:2585–93.
15. Diskin SJ, Hou C, Glessner JT, et al. Copy number variation at 1q21.1 associated with neuroblastoma. Nature 2009;459:987–91.
16. Mosse YP, Laudenslager M, Longo L, et al. Identification of ALK as a major familial neuroblastoma predisposition gene. Nature 2008;455:930–5.
17. Weiss WA, Aldape K, Mohapatra G, Feuerstein BG, Bishop JM. Targeted expression of MYCN causes neuroblastoma in transgenic mice. EMBO J 1997;16:2985–95.
18. Hansford LM, Thomas WD, Keating JM, et al. Mechanisms of embryonal tumor initiation: distinct roles for MycN expression and MYCN amplification. Proc Natl Acad Sci U S A 2004;101:12664–9.
19. Chesler L, Goldenberg DD, Seales IT, et al. Malignant progression and blockade of angiogenesis in a murine transgenic model of neuroblastoma. Cancer Res 2007;67:9435–42.
20. Wang Q, Diskin S, Rappaport E, et al. Integrative genomics identifies distinct molecular classes of neuroblastoma and shows that multiple genes are targeted by regional alterations in DNA copy number. Cancer Res 2006;66:6050–62.
21. Thomas PD, Campbell MJ, Kejariwal A, et al. PANTHER: a library of protein families and subfamilies indexed by function. Genome Res 2003;13:2129–41.
22. Fredlund E, Ringner M, Maris JM, Pahlman S. High Myc pathway activity and low stage of neuronal differentiation associate with poor outcome in neuroblastoma. Proc Natl Acad Sci U S A 2008.
23. Zeller KI, Jegga AG, Aronow BJ, O'Donnell KA, Dang CV. An integrated database of genes responsive to the Myc oncogenic transcription factor: identification of direct genomic targets. Genome Biol 2003;4:R69.
24. Cole KA, Attiyeh EF, Mosse YP, et al. A functional screen identifies miR-34a as a candidate neuroblastoma tumor suppressor gene. Mol Cancer Res 2008;6:735–42.
25. Whitfield ML, George LK, Grant GD, Perou CM. Common markers of proliferation. Nat Rev Cancer 2006;6:99–106.
26. Van Roy N, De Preter K, Hoebeeck J, et al. The emerging molecular pathogenesis of neuroblastoma: implications for improved risk assessment and targeted therapy. Genome Med 2009;1:74.

27. Hackett CS, Hodgson JG, Law ME, et al. Genome-wide array CGH analysis of murine neuroblastoma reveals distinct genomic aberrations which parallel those in human tumors. Cancer Res 2003;63:5266–73.
28. Sweet-Cordero A, Mukherjee S, Subramanian A, et al. An oncogenic KRAS2 expression signature identified by cross-species gene-expression analysis. Nat Genet 2005;37:48–55.
29. Louis SF, Vermolen BJ, Garini Y, et al. c-Myc induces chromosomal rearrangements through telomere and chromosome remodeling in the interphase nucleus. Proc Natl Acad Sci U S A 2005;102:9613–8.
30. Yamamoto Y, Sakamoto M, Fujii G, et al. Overexpression of orphan G-protein-coupled receptor, Gpr49, in human hepatocellular carcinomas with β-catenin mutations. Hepatology 2003;37:528–33.
31. Tanese K, Fukuma M, Yamada T, et al. G-protein-coupled receptor GPR49 is up-regulated in basal cell carcinoma and promotes cell proliferation and tumor formation. Am J Pathol 2008;173:835–43.
32. McClanahan T, Koseoglu S, Smith K, et al. Identification of overexpression of orphan G protein-coupled receptor GPR49 in human colon and ovarian primary tumors. Cancer Biol Ther 2006;5:419–26.
33. Musacchio A, Salmon ED. The spindle-assembly checkpoint in space and time. Nat Rev Mol Cell Biol 2007;8:379–93.
34. Wood KW, Chua P, Sutton D, Jackson JR. Centromere-associated protein E: a motor that puts the brakes on the mitotic checkpoint. Clin Cancer Res 2008;14:7588–92.
35. Hu ZKW, Das D, Ziyad S, et al. Small molecular inhibitory of the centromere-associated protein E (CENP-E), GSK923295A inhibits cell growth in breast cancer cells. AACR: Denver (CO); 2009.